Scintigraphic Detection of Melanoma Metastases with a Radiolabeled Benzamide ([Iodine-123]-(S)-IBZM)

Lorenzo Maffioli, Luigi Mascheroni, Valeria Mongioj, Massimo Gasparini, Maria Teresa Baldini, Ettore Seregni, Maria Rita Castellani, Natale Cascinelli and GianLuigi Buraggi

Nuclear Medicine Department, Surgical Oncology "B" Department, Health Physics Division, National Cancer Institute, Milan, Italy

Iodine-123-(S)-2-hydroxy-3-iodo-6-methoxy-N-[(1-ethyl-2-pyrrolidinyl) methyl] benzamide ([^{123}I]-(S)-IBZM) is a radiolabeled benzamide usually employed to study neuropsychiatric disorders, such as schizophrenia and Parkinson's disease. The ectodermic origin of melanocytes and the presence of melanin in the substantia nigra are the theoretic basis of the experimental use of this class of tracers for melanoma imaging. **Methods:** Eleven patients with proven metastatic melanoma entered the study. Whole-body and planar scintigrams were performed 2, 4 and 24 hr after intravenous injection of a mean tracer activity of 205 MBq. The dosimetric evaluation was performed by the Medical Internal Radiation Dose Committee method. **Results:** The [^{123}I]-(S)-IBZM scans allowed the detection of all six cutaneous lesions, five of six superficial pathologic lymph nodes, four of five pulmonary and one of two hepatic metastases. The maximum tumor-to-background ratio was 2.6 in planar images. The hepatobiliary excretion of the tracer may limit detection of intra-abdominal lesions. Dosimetry is similar to data for nononcologic patients. **Conclusion:** Although it is unclear if the mechanism of radiopharmaceutical uptake in melanoma is due to binding to membrane receptors or due to interactions with intracellular structures, radiolabeled benzamide is a promising tracer to detect melanoma.

Key Words: melanoma; IBZM; dopamine receptors; tumor imaging

J Nucl Med 1994; 35:1741–1747

The number of new reported cases of malignant melanoma is still increasing. Early diagnosis and accurate follow-up of these patients is of primary importance. The staging and follow-up procedures include physical examination, standard chest radiographs and liver ultrasonography, but in some circumstances, these procedures do not allow the detection of lymph node and visceral metastases.

For this reason, other diagnostic techniques have been proposed. Among them, radioimmunoscintigraphy with radiolabeled monoclonal antibodies directed against melanoma-associated antigens (MAA) has been extensively performed and tested in multicenter trials. Good diagnostic accuracy has been demonstrated (1–3).

Another approach is based on the capacity of the tumor to produce melanin. Several molecules, such as chloroquine and its radiolabeled analogs (iodoquine and iodochloroquine), are taken up by and have been proved to remain present in melanin-containing cells. These drugs thereby bind to preformed melanin. A scintigraphic approach to melanoma detection with these reagents was made in the 1970s (4,5). The major drawback of this technique is due to the normal binding of these reagents to all melanin-containing cells (including normal tissues, such as ocular uvea and skin) (6,7).

Because tyrosine is a melanin precursor, radiolabeled derivatives of this compound (e.g., iodinated alpha-methyltyrosine) (8) have also been tested for melanoma imaging because it is known that this tumor often displays a high rate of melanin synthesis. In addition, numerous attempts have been made to synthesize "false precursors" of melanin, for example, thioamides (thiouracil and its derivatives) (9–11). However, none of these radiopharmaceuticals was successful in the detection of malignant melanomas.

A new class of compounds that seems to show interesting properties is the group of benzamides. These tracers have been synthesized to provide specific imaging of the structures of the brain with a high expression of dopaminergic receptors (basal ganglia) (12).

The ectodermic origin of melanocytes and the presence of melanin in the substantia nigra are the theoretic bases for the application of benzamides in the scintigraphic evaluation of melanoma in humans (13,14). Preliminary results on the use of a tracer of this group ([^{123}I] N-(2-diethylaminoethyl) 4-iodobenzamide (BZA) were recently presented by Michelot et al. and Brandau et al. in patients with cutaneous and ocular melanomas (15–17).

Patient	Age (yr)	Sex	Site of the lesion	Size (mm)
CS-01	62	M	Thigh (4 in-transit metastases)	10–24
BR-02	67	F	Leg	10
DP-03	82	F	Right inguinal lymph nodes	70
MG-04	81	F	Gluteal region	70
MS-05	65	F	In-transit metastases in left hand	15
			Left axillary lymph nodes	10
PL-06	59	F	Intramammary	100
GS-07	41	M	Subclavicular region	50
			Left axillary lymph nodes	25
FG-08	68	M	Left axillary lymph nodes	10
MG-09	51	M	Liver	10–20
CA-10	26	F	Lung	15–40
GA-11	36	M	Bone (vertebrae, femurs)	10–30
			Lung	35
			Mediastinal lymph nodes	25–30

The aim of this study was to evaluate the possibility of using [^{123}I]-(S)-2-hydroxy-3-iodo-6-methoxy-N-[(1-ethyl-2-pyrrolidinyl) methyl] benzamide ([^{123}I]-(S)-IBZM), a tracer usually employed for the study of neuropsychiatric disorders (e.g., Parkinson's disease, schizophrenia, progressive supranuclear palsy and multiple system atrophy), to detect melanomatous lesions in humans.

MATERIALS AND METHODS

Tracer

Iodine-123-(S)-IBZM) is a radiopharmaceutical synthesized by de Paulis et al. (18) and subsequently proposed by Kung et al. (19,20) for the imaging of dopamine D_2 receptors with a traditional gamma camera instead of the expensive and high-technology PET systems. The tracer is the commercially available liquid solution produced by Cygne BV (Eindhoven, The Netherlands)-DuPont Pharma Italia. The radiopharmaceutical had a specific activity greater than 1.85·10^8 GBq/mole, (mean activity concentration = 74 MBq/ml). Quality control procedures performed with thin-layer chromatography showed values of radiochemical purity of more than 97%. A mean dose of 205 MBq of the tracer was slowly injected into the antecubital veins of the patients.

Patients

Eleven patients with histologically proven metastatic melanoma entered the study. The aim of the study was to verify the effective possibility of imaging metastatic melanoma with radio-labeled benzamides.

The main characteristics of the patients are shown in Table 1. Short details about their clinical history are summarized in Appendix A. In their clinical history, all patients had undergone surgical treatment of a primary cutaneous melanoma. At the moment of scintigraphy, they showed one or more lesions, which were clinically and instrumentally (with ultrasonography, radiography, CT or MRI) documented as indicating the presence of melanoma metastases. Six of the discovered lesions were cutaneous, and six were lymph node metastases. Three patients had pulmonary localizations, and two presented also had hepatic metastases. The dimensions of the lesions ranged between 5 and 100 mm. Except for the lung and liver metastases, all lesions were

surgically removed within a few days (1–4 days) after scintigraphy, and histopathologic analysis was performed to confirm the nature of the lesions. To reduce the thyroidal uptake of radio-iodine, the gland was blocked with potassium perchlorate (400 mg orally) 30 min before the radioactive drug was injected.

Scintigraphic Technique

Imaging was performed 2, 4 and in some cases 24 hr after the injection with a dual-head, large-field gamma camera (Sopha DSX Bodytrack, Buc Cedex, France) equipped with an ultrahigh-resolution collimator for low energies. Whole-body scans were acquired with a constant speed of 15 cm·min^{-1}. Regional planar images were fitted over the lesions and acquired for 10 min with a matrix of 256 × 256 (zoom = 1.00, pixel dimension = 2.24 mm).

SPECT was performed in each patient (matrix = 64 × 64, 30 sec/step, 64 steps over 360°; zoom = 1.14, pixel dimension = 7.84 mm). Transaxial images were reconstructed by filtered backprojection with a Hamming/Hann filter characterized by a cutoff frequency of 0.5 cycles/pixel (a low-pass filter useful for medium-noise level images). No attenuation and scatter correction were made.

For radiation dosimetry, we applied the method proposed by the Medical Internal Radiation Dose (MIRD) Committee (Appendix B).

Blood Clearance and Biodistribution Evaluation

Radiopharmaceutical kinetic and biodistribution studies were performed in only three cooperating patients. In regard to the study of the tracer's biodistribution, regions of interest (ROIs) were drawn on digital whole-body images 0, 1, 2, 4 and 6 hr after the injection, which surrounded the brain, lungs, liver and gall-bladder. The percentage activity in the organs at any time was obtained by the following formula:

$$\frac{(\text{geometric mean counts in organ}) \times 100}{(\text{geometric mean counts in whole body at t = 0})^*}$$

The blood clearance was determined by venous samples taken at 5, 10, 15, 20, 30, 60, 90, 180, 240, 360 and 420 min. The total blood volume was estimated by means of a formula based on body weight and height (21). The clearance at any time was expressed as a percentage of the injected activity.

Tumor-to-Background Ratio Evaluation

A semiquantitative analysis was performed to define the best tumor-to-background (T/B) ratios, using the ROI method. An important problem in regard to accurate quantitation of tumor uptake is due to the finite point response function of the gamma camera, i.e., the image of the lesion is larger than its true physical size. If the ROI is reduced to the physical dimension of the lesion, not all counts are included. However, if the ROI is made larger, there will be a significant contribution of counts from adjacent normal tissues. To overcome this difficulty and also to minimize the interobserver variability, the tumor uptake was studied by drawing isocontour ROIs around lesions.

A manual ROI was drawn to define the whole tumor area. With respect to the highest count pixel in the ROI, a threshold (percent of the maximum) was fixed. All pixels with values greater than this threshold were attributed to the first area. Another four areas were created by varying the threshold (20%, 40%, 50% and 60% of the maximum). In this way, five different ROIs were obtained for each tumor.

Background ROIs were drawn near the tumor or in a contralateral region to estimate the binding of the agent and the image contrast of the lesion. Every time, T/B ratios were calculated by dividing the total counts contained in each tumor ROI by the total counts in the background ROI to account for the different number of pixels in the different ROIs.
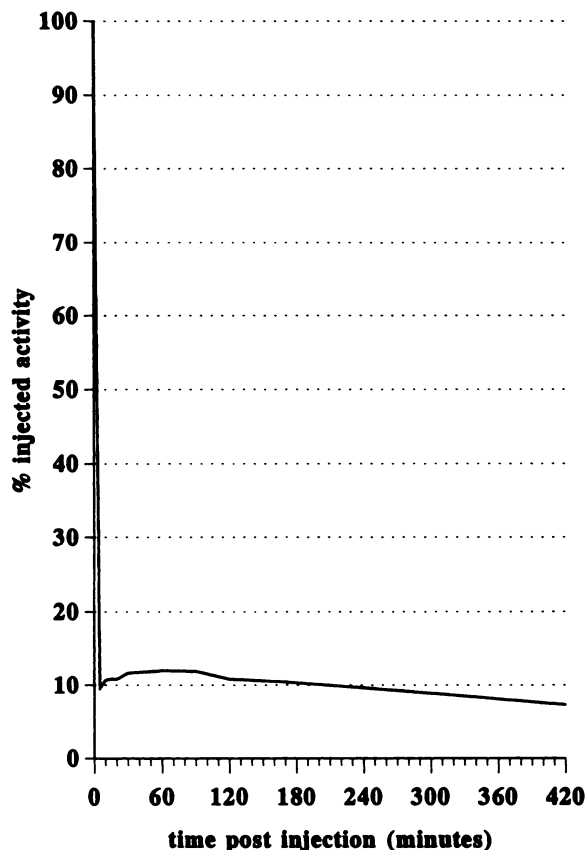

FIGURE 1. Blood clearance curve of [¹²³I]-(S)-IBZM. Tracer rapidly disappears from blood pool. Less than 10% of total injected activity is present 5 min after injection.
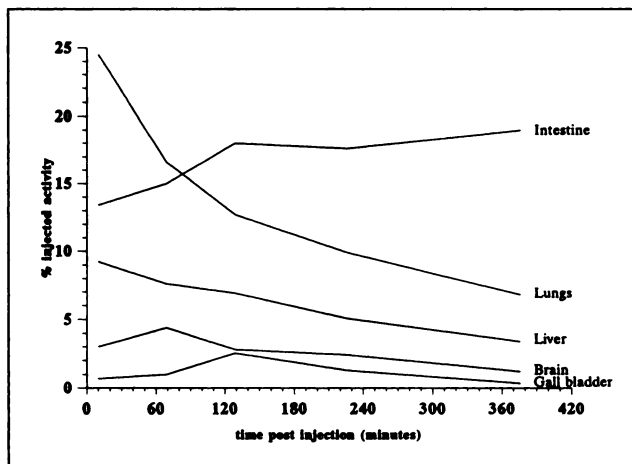

FIGURE 2. Time-activity curves in several organs after intravenous administration of [¹²³I]-(S)-IBZM. Values are expressed as the percentage of total injected activity and corrected for physical decay.

RESULTS

Neither immediate nor delayed side effects were noted after the administration of the radiopharmaceutical. No cerebral lesions were present in the patients evaluated, and no pathologic uptake was documented in the SPECT studies of the brain. The basal ganglia were normally imaged because of the high selectivity of [¹²³I]-(S)-IBZM for D_2 receptors.

After intravenous administration, the tracer is rapidly cleared from the blood pool. Figure 1 shows that, after 5 min, only about 10% of the injected activity is still circulating. Between the first and second hour after the injection, there is a slight increase in blood activity, which lasts for 1 hr. Thereafter, a slow but continuous decrease characterizes the remaining curve.

Images and biodistribution data indicate a relatively high concentration of the compound in lungs, liver and gallbladder. The hepatobiliary excretion of the tracer is due in part to the high lipophilicity of the compound and explains the presence of its high activity in the intestinal tract. The time-activity curves plotted in Figure 2 show that 24.5% of the injected activity is in the lungs and 9% is in the liver 10 min after administration. At 6 hr, the activity in these organs has dropped to 6.8% and 3.4%, respectively. During this interval, the intestinal activity rises. The activity in the brain increases from 3% at 10 min to 4% at 1 hr and decreases to 1.2% at 6 hr. Although all patients were given potassium perchlorate, some thyroid uptake was observed in many patients.

Table 2 shows the clinical results of this study. The IBZM scan allowed the detection of all cutaneous lesions and of five of six superficial pathologic lymph nodes (Figs. 3, 4, 5). The false-negative case was a small (1 cm) axillary adenopathy. The lesion's dimensions (close to the spatial resolution of the system) and the low lesion-to-background concentration ratios were the main factors that affected the imaging.

TABLE 2
Overall Results

Sites of disease	Presence of disease	Lesions detected
Lymph nodes	6	5
Skin	6	6
Lung	5	4
Liver	2	1
Bone	4	4
Total	23	20

With regard to visceral metastases, in spite of the relatively high background activity in the lung and liver, four of five metastases documented with standard chest radiographs were identified in the lungs. One lesion was detected in the liver; this observation was in good agreement with ultrasonographic findings.

The T/B ratios showed that the highest values were obtained 4 hr after injection, with a maximum of 2.6 (Table 3). Increasing values were observed during the first hours and decreasing values in delayed images. For example, for Patient CS-01, we observed a T/B ratio of 1.48 at 30 min after the injection, which was 1.85 and 1.5, respectively, after 3 and 4 hr. In Patient CA-10, we obtained a T/B ratio of 1.54 after the first hour, 1.7 after 3 hr and 1 after 24 hr.

Moreover, when the different threshold ROIs drawn for each tumor were compared, T/B ratio growth was observed in the case of rather small tumor ROIs. This general observation is probably due in part to scatter and in part to possible involutional processes related to intralesional ischemia and necrosis.

Table 4 shows the dosimetry in men and women after intravenous administration of this radiopharmaceutical. The estimated doses to organs were computed with the mathematic method discussed earlier. The highest doses were calculated for lung, liver and gallbladder. The intes-
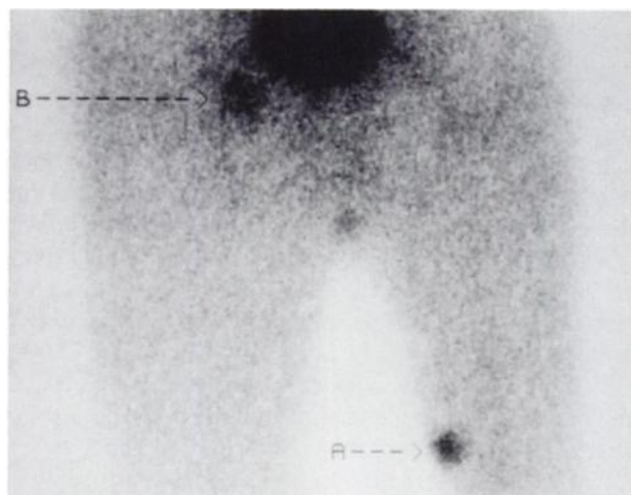

FIGURE 4. Planar scintigraphy of thorax acquired 3 hr after intravenous injection of [^{123}I]-(S)-IBZM. Melanoma metastases are detectable in left lung and mediastinum. Tumor-to-lung ratios are 2.52, 1.34 and 1.30, respectively, for upper, middle and lower lesion.

tinal data were not computed because of the impossibility of obtaining sufficient information about the activity that entered the small intestine, as required by the kinetic model described in ICRP Publication no. 30 (22).

The spleen was not visualized in seven cases. In the remaining four and in delayed images, the splenic uptake was poor. For this reason, absorbed doses (as reported in Table 4) were obtained by evaluating the spleen only as a target organ. Considering the spleen as the source organ, the splenic dose is to be increased by about 50%. The dose in the stomach, kidneys and pancreas has to be increased by about 5%; in the other organs, the dose differences are negligible.

FIGURE 3. Anterior view of pelvis and thighs. Scintigraphy was performed 4 hr after tracer administration. Pathologic uptakes of radiotracer are present in the right thigh (A) and in correspondence to contralateral pelvic lymph nodes (B).
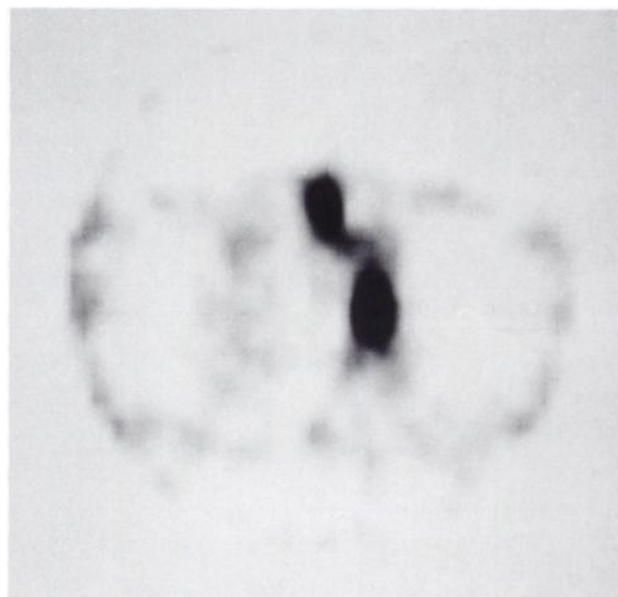

FIGURE 5. Transaxial slice of the SPECT study performed over the chest of the same patient imaged in Figure 4. Intrathoracic lesions show selective uptake of [^{123}I]-(S)-IBZM.

TABLE 3
Tumor-to-Background Ratios with Isocontour Regions of
Interest Drawn with Different Thresholds (%) for Each Patient

Patient	100-0	100-20	100-40	100-50	100-60
CS-01	1.48	1.48	1.54	1.63	1.74
	1.55	1.55	1.55	1.56	1.61
BR-02	1.51	1.51	1.54	1.60	1.61
DP-03	2.20	2.21	2.29	2.44	2.50
MG-04	1.31	1.32	1.35	1.38	1.38
MS-05	1.57	1.78	2.27	2.53	2.60
	1.75	1.81	2.28	2.50	2.59
PL-06	1.23	1.24	1.44	1.67	1.68
GS-07	1.21	1.23	1.31	1.44	1.52
FG-08	1.18	1.20	1.27	1.35	1.36
MG-09	1.52	1.52	1.57	1.61	1.61
CA-10	1.36	1.36	1.36	1.36	1.36
	1.67	1.67	1.67	1.67	1.67
GA-11	2.52	2.52	2.52	2.55	2.66
	1.34	1.34	1.34	1.36	1.39
	1.30	1.30	1.31	1.36	1.44

DISCUSSION

Various attempts have been made in the past to find tracers with a high selectivity for melanoma. Apart from immunoscintigraphy with monoclonal antibodies directed against MAA, other methods (chloroquine and its derivatives, alpha-methyltyrosine and thioamides) do not image this tumor because of poor sensitivity, specificity or unavailability of the radiopharmaceuticals (23).

Iodine-123-(S)-IBZM has a high affinity for dopaminergic D_2 and probably also D_3 receptors. For this reason, it is used in nuclear medicine for the diagnosis and treatment monitoring of several neuropsychiatric disorders (e.g., schizophrenia, Parkinson's disease and Wilson's disease) in which the dopaminergic system is involved. This radiopharmaceutical was selected to detect melanoma metastases in humans on the basis of the ectodermic origin of melanocytes. This is the first report to the authors' knowledge of the use of [123I]-(S)-IBZM in oncology. Other authors [Michelot et al. (15) and Brandau et al. (16)] have recently tested an analog radioio-

TABLE 4
Dosimetry in Men and Women*

Organ	Men	Women
Brain	0.0129	0.0115
Stomach	0.0127	0.0143
Heart wall	0.0132	0.0156
Kidneys	0.0123	0.0134
Liver	0.0157	0.0253
Lungs	0.0247	0.0386
Pancreas	0.0144	0.0162
Red marrow	0.0116	0.0119
Spleen	0.0125	0.0135
Gallbladder	0.0348	0.0745
Total body	0.0117	0.0125

*Averages expressed in mGy/MBq

dinated benzamide (BZA) in animals and humans to evaluate the presence of melanoma metastases.

The tumor uptake of [123I]-(S)-IBZM is evident, but the maximum T/B ratio was never greater than 2.6 in planar images. This result is of the same order as that described by Brandau et al. (16) with 123I-BZA but lower than those reported by Michelot et al. (15) in an animal model (C57BL6 mice bearing B16 melanoma) in which ratios were obtained that ranged between 4.95 (tumor-to-liver) and 146.95 (tumor-to-brain) 24 hr after 125I-BZA administration.

The results obtained in superficial (lymph node and cutaneous) metastasis imaging indicate a good sensitivity for this target. The only undetected lesion was a metastasis 1 cm in diameter, which is close to the spatial resolution of the system. However, the major drawback of the method is related to the hepatobiliary excretion of the [123I]-(S)-IBZM, which leads to a relatively high abdominal activity. In many cases, this factor could obscure the detection of possible intra-abdominal involvement and thus be an important limitation for the clinical staging of the disease.

Although each patient received 400 mg of potassium perchlorate, the images showed some thyroid uptake. This suggests that such pretreatment is in most cases inadequate and should be improved by giving higher doses or by the administration of Lugol's solution.

In regard to the dosimetric results, these were in good agreement with the data in the literature for nononcologic patients and healthy subjects, especially in the brain, stomach, kidneys, pancreas, red marrow, lungs and total body (24,25).

The mechanism of uptake of radiolabeled benzamides by melanoma cells is still not completely defined. However, the fact that increasing values were observed during the first hours and decreasing ones in delayed images may suggest that the uptake is due not only to an increased regional blood flow but is also related to a specific mechanism of uptake, followed by a slow washout from lesions. So, at least two possible pathways can be proposed: (1) a selective binding mediated by specific membrane receptors or (2) a specific interaction with intracellular structures (e.g., melanin or its precursors). The first one is based on the well-known characteristic of this class of molecules to bind to dopaminergic receptors. Unfortunately, to date there is no information about the real presence of this type of receptor on the surface of melanocytes. It would be useful to carry out a study with this aim. The second mechanism could be similar to that demonstrated for chlorpromazine. It has been shown that chlorpromazine is able both to bind D_2 receptors and to react with melanin in the cells. In the latter case, chlorpromazine plays the role of an electron donor to the pigment, which serves as an electron acceptor (26,27). The binding was supposed to be related to the presence of a phenothiazine ring. Based on these considerations, it can be hypothesized also that benzamides could cross the cellular membrane and bind in some way to the melanin. This assumption has been partially confirmed by Michelot (17), who demonstrated that radiola-

beled benzamide ^{123}I-BZA is a valid tracer for the detection of melanotic lesions, whereas the method gives false-negative results in the case of amelanotic tumors. However, if [123I]-(S)-IBZM penetrates nonspecifically into the cells with an intracellular melanin content, all melanin-containing cells (including ocular uvea and skin), as previously found for labeled chloroquine and its analogs, should be visualized. In the experience cited in the article, no [123I]-(S)-IBZM uptake was seen in these elements.

CONCLUSIONS

The tracer [123I]-(S)-IBZM seems to represent a valid improvement in the class of radiopharmaceuticals that shows some sensitivity in the in vivo detection of melanoma metastases. However, a selection of derivatives with higher tumor uptakes (after a clear demonstration of the biochemical processes involved in the cellular uptake in melanoma) and lower lipophilicity (with consequently lower biliary excretion) could be the next effective step.

APPENDIX A

PATIENTS' CLINICAL DATA

CS-01: Surgical excision of melanoma on the left foot, Clark's level III, 2.7-mm thick (August 1983). Chemotherapy. Surgical excision and hyperthermia of a local relapse (November 1984). Excision of four left crural metastatized lymph nodes (November 1985). Amputation of left leg for multiple metastases and chemotherapy (May 1989). Appearance of four lesions on left thigh and contralateral inguinal adenopathy. Brain MRI, liver ultrasound results negative.

BR-02: Surgical excision of melanoma, Clark's level IV, 5.4-mm thick on right leg (May 1991). Subcutaneous relapse in right leg (May 1992).

DP-03: Excision of malignant melanoma on right leg, Clark's level IV, 6.8-mm thick (March 1989). Right inguinal adenopathy (March 1991).

MG-04: Surgical demolition of right outer ear for malignant melanoma, Clark's level V, more than 4-mm thick (November 1980). In July 1992, relapse in subcutaneous right gluteal region. Chest radiographs and liver ultrasound findings negative.

MS-05: Excision of malignant melanoma on left hand (May 1989). Excision of relapse on middle finger of left hand (September 1990). In-transit metastases in left planar region of the left hand and suspected axillary adenopathy.

PL-06: Surgical excision of melanoma from right elbow (June 1987). Excision of local relapse (June 1989). Right axillary lymphadenectomy for relapse (August 1989). Right lung lobectomy for melanoma metastasis in medium lobe (May 1991). Intramammary metastasis (September 1992).

GS-07: Surgical excision of melanoma of the trunk, Clark's level IV, 2.7-mm thick (September 1991). Interferon therapy (December 1991). Bilateral axillary lymphadenectomy (July 1992). Appearance of metastases in subclavear region and in left axilla.

FG-08: Surgical excision of melanoma of the trunk, Clark's level IV, 4.2-mm thick (April 1992). Left axillary adenopathy (August 1992).

MG-09: Excision of melanoma in the trunk, Clark's level V, 2-cm thick (June 1988). Appearance of multiple hepatic metastases.

CA-10: Excision of melanoma from right shoulder (May 1988). Right axillary lymphadenectomy (September 1989). Dissection of right lower pulmonary lobe for metastases (April 1991). New bilateral lung metastases.

GA-11: Diagnosis of C3 pathologic fracture treated with radiotherapy (July 1993). Detection of left pulmonary mass. Bronchoscopy. Histologic finding of melanoma metastasis. Detection of multiple metastases (skin, lymph nodes and bones).

APPENDIX B

DOSIMETRIC CALCULATIONS

The brain, liver, lungs and gallbladder were considered as source organs. According to the MIRD method (28,29), the absorbed dose to a target organ (r_k) from a single source organ (r_h) is

$$D_k = \bar{A} \cdot S(r_k \leftarrow r_h),$$

where D_k = absorbed dose to target organ [Gy], $\bar{A}$ = cumulated activity in source organ [MBq·hr] and $S(r_k \leftarrow r_h)$ = absorbed dose to target organ per unit cumulated activity in source organ (Gy/MBq · hr).

The cumulated activity is calculated using the time-activity curve generated from organ ROI analysis, and S values are obtained from MIRD tables (standard man phantom for male and 15-yr-old phantom for female).

The whole-body dose is given by:

$$D_{wb} = \bar{A} \cdot S(wb \leftarrow wb),$$

where $\bar{A}$ is obtained from the whole-body retention measurements.

The total dose to a target organ is given by:

$$D_k = \sum_h \bar{A}_h \cdot S(r_k \leftarrow r_h) + \bar{A}_{RB} \cdot S(r_k \leftarrow RB),$$

where the first term represents the dose to the target caused by the activity in source organs, and the second refers to the dose to the target as a result of the activity in remaining body (RB) (22,30).

ACKNOWLEDGMENTS

REFERENCES

1. Buraggi GL, Callegaro L, Mariani G, et al. Imaging with ^{131}I-labeled monoclonal antibodies to a high molecular weight melanoma associated antigen in patients with melanoma: efficacy of whole immunoglobulin and its F(ab')₂ fragments. Cancer Res 1985;45:3378-3387.
2. Buraggi GL, Callegaro L, Turrin A, et al. Immunoscintigraphy with ^{123}I, ^{99m}Tc and ^{111}In-labelled F(ab')₂, fragments of monoclonal antibodies to a human high molecular weight melanoma associated antigen. J Nucl Med 1984;28:195-283.
3. Siccardi AG, Buraggi GL, Natali PG, et al. European multicenter study on melanoma immunoscintigraphy by means of ^{99m}Tc-labeled monoclonal antibody fragments. Eur J Nucl Med 1990;16:317-323.
4. Beierwaltes WH, Lieberman LM, Varma VM, Counsell RE. Visualizing human malignant melanoma and metastases. Use of chloroquine analog tagged with iodine-125. JAMA 1968;206:97-102.
5. Dencker L, Lindquist NG, Tjälve H. Uptake of ^{14}C-labelled chloroquine and an ^{125}I-labelled chloroquine analogue in some polypeptide hormone producing cell system. Med Biol 1976;54:62-68.

6. Dencker L, Lindquist NG, Ullberg S. Distribution of an ^{125}I-labelled chloroquine analogue in a pregnant Macaca monkey. *Toxicology* 1975;5:255–265.

7. Lindquist NG, Ullberg S. The melanin affinity of chloroquine and chlorpromazine studied by whole body autoradiography. *Acta Pharmacol Toxicol (Copenh)* 1972;2(suppl 2):1–32.

8. Kloss G, Leven M. Accumulation of radioiodinated tyrosine derivatives in the adrenal medulla and in melanomas. *Eur J Nucl Med* 1979;4:179–186.

9. Dencker L, Larsson B, Olander K, Ullberg S, Yokota M. False precursor of melanin as selective melanoma seekers. *Br J Cancer* 1979;39:449–452.

10. Larsson B, Olander K, Dencker L, Holmqvist L. Accumulation of ^{125}I-labelled thiouracil and propylthiouracil in murine melanotic melanomas. *Br J Cancer* 1982;46:538–550.

11. Whittaker JR. Biosynthesis of a thiouracil pheomelanin in embryonic pigment cells exposed to thiouracil. *J Biol Chem* 1971;246:6217–6226.

12. Moreau MF, Madelmont JC, Michelot J, et al. Synthesis and experimental study of new ^{125}I-labeled compounds. Potential application for diagnosis and treatment of malignant melanoma in nuclear medicine. In: Schmidt HAE, Höfer R, eds. *Nuclear medicine. Nuclear medicine in research and practice.* New York: Schattauer; 1992:190–193.

13. Michelot J, Veyre A, Bonafus J, et al. Phase-2 scintigraphic study of malignant melanoma (MM) and metastases with 123-iodine N-(2-diethylaminoethyl) 4-iodobenzamide. In: Schmidt HAE, Höfer R, eds. *Nuclear medicine. Nuclear medicine in research and practice.* New York: Schattauer; 1992:692–694.

14. Maffioli L, Mascheroni L, Clemente C, Baldini M, Castellani MR. [^{123}I]IBZM uptake in metastatic melanoma. *J Nucl Biol Med* 1993;37:18–20.

15. Michelot JM, Moreau MFC, Labarre PG, et al. Synthesis and evaluation of new iodine-125 radiopharmaceuticals a potential tracers for malignant melanoma. *J Nucl Med* 1991;32:1573–1580.

16. Brandau W, Kirchner B, Bartenstein P, et al. N-(2-diethylaminoethyl)-4-[^{123}I]iodobenzamide as a tracer for the detection of malignant melanoma: simple synthesis, improved labelling technique and first clinical results. *Eur J Nucl Med* 1993;20:238–243.

17. Michelot JM, Moreau MFC, Veyre AJ, et al. Phase II scintigraphic clinical trial of malignant melanoma and metastases with iodine-123-N-(2-diethylaminoethyl 4-iodobenzamide). *J Nucl Med* 1993;34:1260–1266.

18. de Paulis T, Kumar Y, Johansson L, et al. Potential neuroleptic agents. 3. Chemistry and antidopaminergic properties of substituted 6-methoxysalicylamides. *J Med Chem* 1985;28:1263–1269.

19. Kung HF, Xu X-J, Guo Y-Z. Preparation and radiolabelling of IBZM: a potential D2 specific brain imaging agent for SPECT. *J Labelled Compd Radiopharm* 1986;23:1318–1319.

20. Kung HF, Pan S, Kung MP, et al. In vitro and in vivo evaluation of [^{123}I]-IBZM: a potential CNS D-2 dopamine receptor imaging agent. *J Nucl Med* 1989;30:88–92.

21. Allen TH. Symposium on nutrition: prediction of blood volume and adiposity in man from body weight and cube of height. *Metabolism* 1956;5:328–345.

22. Sowby ED, ed. *Part I. Limit for intakes of radionuclides by workers.* ICRP publication #30. Oxford: Pergamon Press; 1979.

23. Reisfield RA. Monoclonal antibodies as probes for structure and function of human melanoma associated antigens. In: Veronesi U, Cascinelli N, Santinami M, eds. *Cutaneous melanoma.* London: Academic Press; 1987:374–379.

24. Kung HF, Alavi A, Chang W, et al. In vivo SPECT imaging of CNS D-2 dopamine receptors: initial studies with iodine-123-IBZM in humans. *J Nucl Med* 1990;31:573–579.

25. Cygne BV. *123I-(S)-IBZM product specifications. Properties, potential clinical applications.* Eindhoven: Cygne BV; July 1992.

26. Bolt AG, Forrest IS. Interaction between human melanoprotein and chlorpromazine derivatives. II. Spectro-photometric studies. *Life Sci* 1967;6:1258–1292.

27. Fairchild RG, Greenberg D, Watts KP, et al. Chlorpromazine distribution in hamsters and mice bearing transplantable melanoma. *Cancer Res* 1982;42:556–562.

28. Snyder WS, Ford MR, Warner GG, Watson SB. "S", absorbed dose per unit cumulated activity for selected radionuclides and organs. MIRD pamphlet # 11. New York: The Society of Nuclear Medicine; 1975.

29. Loevinger R, Budinger TF, Watson EE. *MIRD primer for absorbed dose calculations.* New York: The Society of Nuclear Medicine; 1988.

30. Cloutier RJ, Watson EE, Rohrer RH, Smith EM. Calculating the radiation dose to an organ. *J Nucl Med* 1973;14:53–55.